

# Nonlinear Quantum Rabi Model in Trapped Ions

Xiao-Hang Cheng,<sup>1,2</sup> Iñigo Arrazola,<sup>2</sup> Julen S. Pedernales,<sup>2,3</sup> Lucas Lamata,<sup>2</sup> Xi Chen,<sup>1</sup> and Enrique Solano<sup>2,4</sup>

<sup>1</sup>*Department of Physics, Shanghai University, 200444 Shanghai, People's Republic of China*

<sup>2</sup>*Department of Physical Chemistry, University of the Basque Country UPV/EHU, Apartado 644, 48080 Bilbao, Spain*

<sup>3</sup>*Institute for Theoretical Physics and IQST, Albert-Einstein-Allee 11, Universität Ulm, D-89069 Ulm, Germany*

<sup>4</sup>*IKERBASQUE, Basque Foundation for Science, Maria Diaz de Haro 3, 48013 Bilbao, Spain*

(Dated: May 16, 2022)

We study the nonlinear dynamics of trapped-ion models far away from the Lamb-Dicke regime. This nonlinearity induces a sideband cooling blockade, stopping the propagation of quantum information along the Hilbert space of the Jaynes-Cummings and quantum Rabi models. We compare the linear and nonlinear cases of these models in the ultrastrong and deep strong coupling regimes. Moreover, we propose a scheme that simulates the nonlinear quantum Rabi model in all coupling regimes. This can be done via off-resonant nonlinear red and blue sideband interactions, yielding applications as a dynamical quantum filter.

PACS numbers: 03.67.Ac, 03.67.Lx, 37.10.Ty, 42.50.Ct, 37.10.Vz

*Introduction.*—Proposed in 1936 by I. I. Rabi [1], the most fundamental interaction between a two-level atom and a classical light field, the semiclassical Rabi model, has played an important role in both physics and mathematics [2, 3]. Under the rotating wave approximation (RWA), its fully quantized form, the quantum Rabi model (QRM), can be reduced into the Jaynes-Cummings model (JCM) [4], which is analytically solvable [5]. This model describes the basic interaction in trapped ions [6], superconducting circuits [7], and cavity quantum electrodynamics [8], when the systems are in the regime where the ratio of coupling strength  $g$  and mode frequency  $\nu$  is approximately smaller than 0.1 [9]. On the other hand, in the ultrastrong coupling (USC) regime,  $g/\nu \in (0.1, 1)$  [10, 11], and deep strong coupling (DSC) regime ( $g/\nu > 1$ ) [12–14], we have to take the counter rotating term that is neglected in the JCM into account. The QRM is a fruitful physical model with applications in condensed matter, quantum optics, and quantum information processing. In fact, the QRM has been investigated in many contexts, such as quantum phase transitions (QPT) [15–17], dissipative QRM [18], generalized QRM [19–22], multiparticle QRM [23–26], and quantum thermodynamics [27], among others. Furthermore, proposals and experimental realizations of the QRM in different quantum simulators as optical lattices [28], circuit QED [29], as well as trapped ions [30–32] have been put forward. Reference [30] introduced an analog method for the simulation of different regimes of the QRM, otherwise inaccessible to experimentation from first principles.

As one of the most controllable quantum systems, trapped ions play an important role in diverse proposals for quantum simulations [30, 33–46]. However, most of these works are based on the condition for the system to be in the Lamb-Dicke (LD) regime. In this regime, the wavelength associated to the ion is much smaller than that of the external light, such that the coupling between the internal and the vibrational degrees of freedom can be approximated to first order [6].

In this article, we study the nonlinear effect in a

trapped-ion quantum platform when it is far away from the LD regime. In the past, research in trapped ions beyond the LD regime was mainly focussed on the nonlinear JCM [47–52]. To set up the stage for a subsequent analysis, we first briefly review the JCM and take this as a reference to show the difference with the nonlinear JCM. The appearance of nonlinear terms in the Hamiltonian suppresses the collapses and revivals for a coherent state evolution typical from linear cases. Later on, we investigate single-ion sideband cooling in the nonlinear JCM. The nonlinear term stops the propagation of the open dynamics and further cooling at Fock state  $|n\rangle$ , generating the corresponding  $n$ -phonon Fock state. This can be a useful method to produce high-phonon-number Fock states in a robust way, namely, without specific timings or pulse shapes, and for arbitrary initial motional states, including thermal states. Furthermore, we propose the quantum simulation of the nonlinear quantum Rabi model by simultaneous off-resonant nonlinear Jaynes-Cummings and anti-Jaynes-Cummings interactions. We finally unveil the possibility for the quantum Rabi model to act as a motional state filter.

*Linear and Nonlinear Jaynes-Cummings Model.*—The Hamiltonian describing a two-level trapped ion driven by a monochromatic laser field is expressed as ( $\hbar = 1$ )

$$H = \frac{\omega_0}{2} \sigma_z + \nu a^\dagger a + \frac{\Omega}{2} (\sigma^+ + \sigma^-) [e^{i(kx - \omega t + \phi)} + \text{H.c.}], \quad (1)$$

where  $\omega_0$  is the qubit transition frequency,  $\sigma_z, \sigma^+, \sigma^-$  are spin operators associated to the two-level system,  $\nu$  is the frequency of the harmonic oscillator potential,  $a^\dagger(a)$  is the creation (annihilation) operator associated to the vibrational mode on one direction,  $\Omega$  is the Rabi frequency,  $k$  is the wave number of the external laser field,  $\omega$  is the driving laser frequency, and  $\phi$  is the phase of the laser field.

In the Lamb-Dicke regime,  $\eta \sqrt{\langle (a + a^\dagger)^2 \rangle} \ll 1$ , and after the application of the so-called optical RWA, the

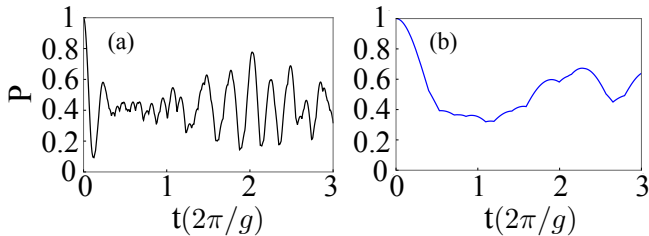


FIG. 1: (color online) Probability versus time of a coherent initial state  $|\alpha = 2\rangle$  after (a) linear JC and (b) NJC evolution. As shown in (a), there exists an approximate collapse and revival in the JCM, while in the NJCM, it vanishes.

Hamiltonian in Eq.(1) can be written as [6]

$$H_{\text{int}}^{\text{LD}} = \frac{\Omega}{2}\sigma^+[1 + i\eta(ae^{-i\nu t} + a^\dagger e^{i\nu t})]e^{i(\phi - \delta t)} + \text{H.c.},$$

where  $\delta = \omega - \omega_0$  is the laser detuning and  $\eta = k\sqrt{\hbar/2M\nu}$  the Lamb-Dicke parameter, with  $M$  the mass of the ion. When  $\delta = -\nu$ , under the vibrational RWA, one obtains the Jaynes-Cummings Hamiltonian,  $H_{\text{JC}} = ig(\sigma^+ a - \sigma^- a^\dagger)$ , where  $g = \eta\Omega/2$ .

Instead, when the system is beyond the Lamb-Dicke regime, the interaction Hamiltonian after applying the optical RWA reads

$$H_{\text{int}} = \frac{\Omega}{2}\sigma^+ e^{i\eta(a^+ e^{i\nu t} + a e^{-i\nu t}) - i(\delta t - \phi)} + \text{H.c.}, \quad (2)$$

and when  $\delta = -k\nu$ , and after applying the vibrational RWA, the  $k$ -quantum nonlinear Jaynes-Cummings model is obtained [47]. For  $k = 1$ , the Hamiltonian reads

$$H_{\text{nJC}} = ig(\sigma^+ f_1(a^\dagger a)a - \sigma^- a^\dagger f_1(a^\dagger a)), \quad (3)$$

where the nonlinear function  $f_1$  [47, 55] is given by

$$f_1(a^\dagger a) = e^{-\eta^2/2} \sum_{l=0}^{\infty} \frac{(-\eta^2)^l}{l!(l+1)!} a^{\dagger l} a^l. \quad (4)$$

We observe approximate collapses and revivals for an initial coherent state with an average number of photons of  $|\alpha|^2 = 4$  by evolving with the JCM, as shown in Ref. [53], see Fig. 1a. Here, we plot the probability  $P(t) = |\langle\psi(0)|\psi(t)\rangle|^2$ . Comparing the same case for the nonlinear JCM, as depicted in Fig. 1b, we appreciate that in the latter case the collapses and revivals vanish, and the dynamics is more irregular. This can seem natural given that the phenomenon of revival takes place whenever the most significant components of the quantum state, after some evolution time, turn out to oscillate in phase again, which may be more unlikely if the dynamics is nonlinear.

*Nonlinear Jaynes-Cummings Model for Sideband Cooling*— To study sideband cooling in both the linear and nonlinear JCM, we introduce a spontaneous decay

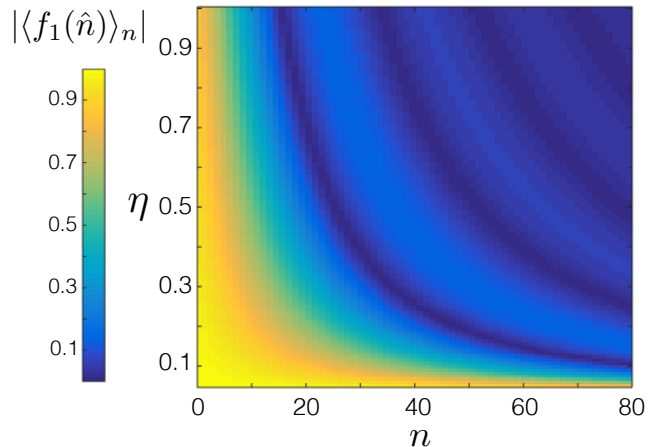


FIG. 2: (color online) The absolute value of the operator  $f_1(a^\dagger a)$  evaluated for different Fock states  $|n\rangle$  and LD parameters  $\eta$ . Dark blue regions represent cases where  $f_1(a^\dagger a)|n\rangle \sim 0$ .

probability in the model, characterized by  $\Gamma_m$ . To calculate the evolution of such a system, we use the master equation,

$$\dot{\rho} = -i[H_{\text{nJC}}, \rho] + \Gamma_m L(\sigma^-)\rho, \quad (5)$$

where the Lindblad superoperator is  $L(\hat{X})\rho = (2\hat{X}\rho\hat{X}^\dagger - \hat{X}^\dagger\hat{X}\rho - \rho\hat{X}^\dagger\hat{X})/2$ .

Sideband cooling beyond the LD limit has been studied years ago [48, 52] for two and more ions by quantum Monte Carlo [54] calculations. At variance with former research, here we show that the dynamics for a single-ion cooling will be totally stopped at Fock state  $|n\rangle$  when the nonlinear term  $f_1(a^\dagger a)|n\rangle = 0$  (See Fig. 2). In other words, one can robustly obtain large, final, target Fock states by a tunable LD parameter. Here, by robust, we mean that we do not need to tune the timings and Rabi frequencies profiles very accurately, given that the whole wavefunction, for an arbitrary initial state with motional components larger than  $n$ , will converge to Fock state  $|n\rangle$  in this case. For comparison, we show survival probabilities of different Fock states for both the JCM and NJCM in Figs. 3 and 4. We see that one can reach the ground state via sideband cooling in the LD limit (magenta line in Fig. 3(a)) when the initial state is  $|7, g\rangle$ . However, the dynamics stops at  $|4, g\rangle$  (red line in Fig. 4(a)) when  $f_1(a^\dagger a)|3\rangle = 0$  ( $\eta = 0.9673$ ) in nonlinear sideband cooling. Thus, one can efficiently generate the target Fock state, which is  $|4, g\rangle$  in the present example.

*Quantum simulation of the nonlinear Rabi model.*— Here we propose to implement the nonlinear Rabi model in all its parameter regimes via the use of the Hamiltonian of Eq.(2). We consider off-resonant first-order red- and blue-sideband drivings with the same coupling  $\Omega$  and corresponding detunings  $\delta_r, \delta_b$ . The interaction Hamil-

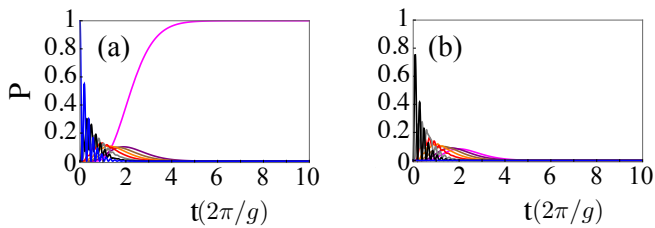


FIG. 3: (color online) Probability versus time for each Fock state with spin down (a) and spin up (b) when the initial state is  $|7, g\rangle$  in a typical sideband cooling system with decay  $\Gamma_m = g$ . Magenta:  $|0\rangle$ , Purple:  $|1\rangle$ , Brown:  $|2\rangle$ , Orange:  $|3\rangle$ , Red:  $|4\rangle$ , Gray:  $|5\rangle$ , Black:  $|6\rangle$ , Blue:  $|7\rangle$ .

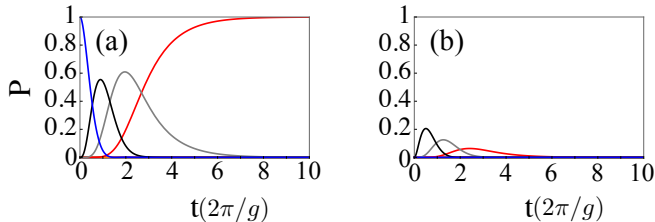


FIG. 4: (color online) Probability versus time for each Fock state in spin down (a) and spin up (b) when the initial state is  $|7, g\rangle$  in a nonlinear sideband cooling system where decay  $\Gamma_m = g$ . The dynamics stops at  $|4, g\rangle$  and leads to the failure of sideband cooling because of the motional barrier provided by  $f_1(a^\dagger a)|3\rangle = 0$ . Magenta:  $|0\rangle$ , Purple:  $|1\rangle$ , Brown:  $|2\rangle$ , Orange:  $|3\rangle$ , Red:  $|4\rangle$ , Gray:  $|5\rangle$ , Black:  $|6\rangle$ , Blue:  $|7\rangle$ .

tonian after optical RWA reads [6, 30],

$$H_{\text{int}} = \sum_{n=r,b} \frac{\Omega}{2} \sigma^+ e^{i\eta} e^{i\nu t} + a e^{-i\nu t} e^{-i(\delta_n t - \phi_n)} + \text{H.c.}, \quad (6)$$

where  $\omega_r = \omega_0 - \nu + \delta_r$  and  $\omega_b = \omega_0 + \nu + \delta_b$  ( $\delta_r, \delta_b \ll \nu \ll \omega_0$ ). We consider the system beyond Lamb-Dicke regime and set the laser field phases  $\phi_{r,b} = 0$ . If we invoke the vibrational RWA, i.e. neglect terms that rotate with frequencies of the order of  $\nu$ , the remaining terms read

$$H_{\text{int}} = ig\sigma^+ (f_1 a e^{-i\delta_r t} + a^\dagger f_1 e^{-i\delta_b t}) + \text{H.c.}, \quad (7)$$

where  $f_1 \equiv f_1(a^\dagger a)$  was introduced in Eq.(4). The latter corresponds to an interaction picture Hamiltonian of the nonlinear quantum Rabi model (NQRM) with respect to the free Hamiltonian  $H_0 = \frac{1}{4}(\delta_b + \delta_r)\sigma_z + \frac{1}{2}(\delta_b - \delta_r)a^\dagger a$ . Therefore, undoing the interaction picture transformation, we have

$$H_{\text{nQRM}} = \frac{\omega_0^R}{2} \sigma_z + \omega^R a^\dagger a + ig(\sigma^+ - \sigma^-)(f_1 a + a^\dagger f_1), \quad (8)$$

where  $\omega_0^R = -\frac{1}{2}(\delta_r + \delta_b)$  and  $\omega^R = \frac{1}{2}(\delta_r - \delta_b)$ . Thus, it is possible to achieve this trapped-ion NQRM with simultaneous off-resonant blue and red sidebands, and by controlling the detunings  $\delta_b$  and  $\delta_r$  one may be able to access different coupling regimes of the model, tuning the ratio  $g/\omega^R$  that defines them.

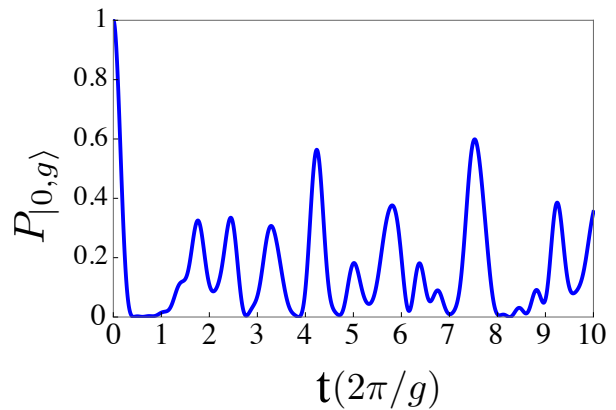


FIG. 5: (color online) Probability versus time of Fock initial state  $|0, g\rangle$  after nonlinear Rabi evolution. We consider red-sideband excitation  $\delta_r = 2\pi \times 11.31\text{kHz}$ , blue-sideband excitation  $\delta_b = -2\pi \times 11.31\text{kHz}$  and coupling strength  $g = 2\pi \times 45.24\text{kHz}$ , with LD parameter  $\eta = 0.67898$ , where  $f_1|7\rangle = 0$ .

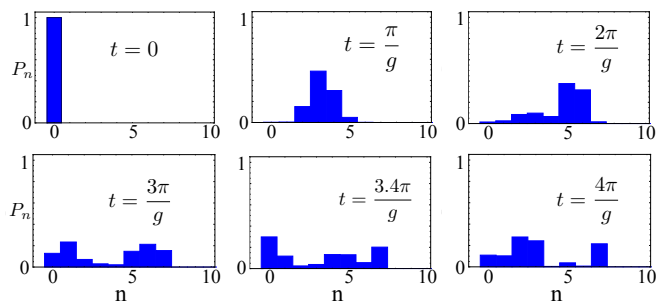


FIG. 6: (color online) Phonon statistics at different times of the nonlinear Rabi model evolved from the initial state  $|0, g\rangle$ . Parameters are the same as those in Fig.5. The whole dynamics stops at  $|n = 7\rangle$  and the Hilbert space is divided into two parts because of the nonlinear term associated with  $f_1|7\rangle = 0$ .

In 1998, Lo suggested that the NQRM in trapped ions is counterintuitive and that the counterrotating terms change the system dramatically [55]. Here, we consider the quantum simulation of this model in arbitrary coupling regimes to unveil possible applications in robust Fock-state generation as well as filtering of the motional states. With this we mean to prevent the motional states to acquire Fock-state population beyond a threshold.

As an example, here we investigate the NQRM in DSC regime with an initial Fock state  $|0, g\rangle$ , where  $|0\rangle$  is the lowest energy state in the harmonic trap and  $|g\rangle$  stands for the ground state of a two-level system. As studied before [12], the linear quantum Rabi model shows collapses and revivals and the round trip of a phonon wavepacket in one period in the DSC regime. On the other hand, in the nonlinear case, Fig. 5 reveals that collapses and revivals do not present the same clear structure, having a more ir-

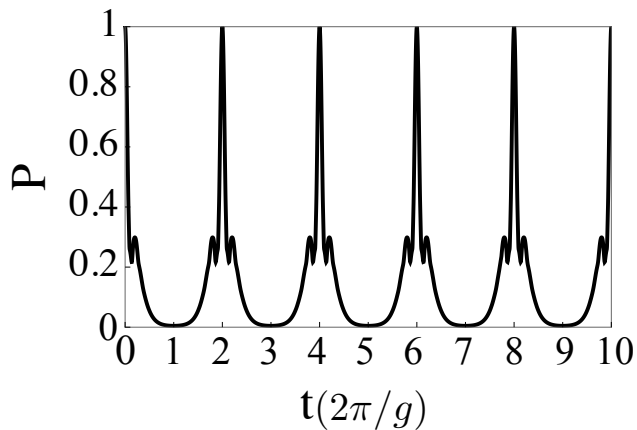


FIG. 7: (color online) Probability versus time of coherent initial state  $|\alpha = 1\rangle$  after linear Rabi evolution. Collapses and revivals appear due to the DSC of the linear QRM. We consider red-sideband excitation  $\delta_r = 2\pi \times 11.31\text{kHz}$ , blue-sideband excitation  $\delta_b = -2\pi \times 11.31\text{kHz}$  and coupling strength  $g = 2\pi \times 22.62\text{kHz}$ .

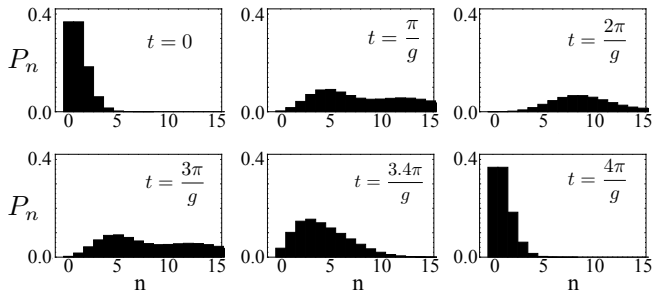


FIG. 8: (color online) Phonon statistics at different times of linear Rabi model evolved from a coherent initial state  $|\alpha = 1\rangle$ . We see the round trip of a phonon number wavepacket in one period.

regular evolution. Most interestingly, the system dynamics never surpasses the Fock state  $|n\rangle$ , wherever we set  $f_1|n\rangle = 0$ . In Fig. 5, we study the case for  $\eta = 0.67898$ ,  $f_1|7\rangle = 0$ ,  $\delta_r = 2\pi \times 11.31\text{kHz}$ ,  $\delta_b = -2\pi \times 11.31\text{kHz}$ ,  $g = 2\pi \times 45.24\text{kHz}$  and  $\Omega = 2\pi \times 133.26\text{kHz}$ . We point out that the nonlinear term also contributes to the coupling strength. Therefore, to keep the NQRM in the DSC regime, the ratio  $g/\omega^R$  should be larger than that for the linear QRM since the nonlinear term  $\langle f_1 \rangle_n$  is always smaller than 1. Summarizing, our result illustrates that the Hilbert space is effectively divided into two parts by the NQRM, and we denote the Fock number  $n$  where  $f_1|n\rangle = 0$  as “the barrier” of the nonlinear Rabi system.

To benchmark the effect of the barrier, we also start to evolve the NQRM system with an initial coherent state with  $\alpha = 1$  whose average phonon number is  $\langle n \rangle = |\alpha|^2 = 1$ , and make the comparison between the QRM and the NQRM in the DSC. The probability of the initial coherent state in the linear QRM performs periodic collapses and full revivals in Fig. 7. In Fig. 8, we observe

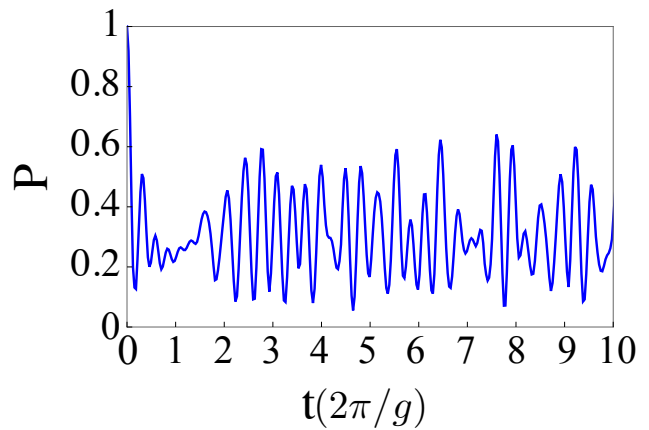


FIG. 9: (color online) Probability versus time of coherent initial state  $|\alpha = 1\rangle$  after nonlinear Rabi evolution. We consider red-sideband excitation  $\delta_r = 2\pi \times 11.31\text{kHz}$ , blue-sideband excitation  $\delta_b = -2\pi \times 11.31\text{kHz}$  and coupling strength  $g = 2\pi \times 41.88\text{kHz}$  when LD parameter  $\eta = 0.57838$  where  $f_1|10\rangle = 0$ .

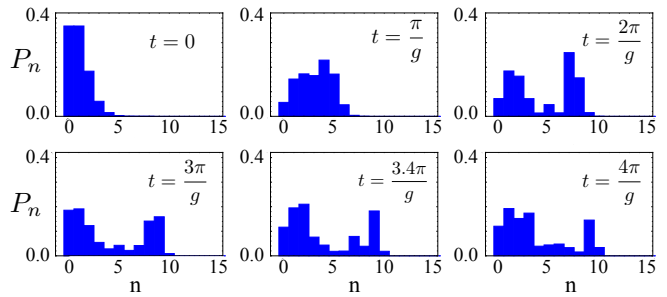


FIG. 10: (color online) Phonon statistics at different times of nonlinear Rabi model evolved from a coherent initial state  $|\alpha = 1\rangle$ . The Fock state with  $n = 10$  is never surpassed because of the nonlinear interaction with  $f_1|10\rangle = 0$ .

the round trip of the phonon wave packet, similarly to the initial Fock state previously studied in Ref. [12]. The NQRM, on the other hand, has an associated dynamics that is aperiodic and more irregular, as shown in Fig. 9, and never crosses the motional barrier produced by the corresponding  $f_1$  zero. Therefore, it can be employed as a motional filter, which is determined by the location of the barrier with respect to the initial state distribution. Here, we choose the LD parameter  $\eta = 0.57838$  with  $f_1|10\rangle = 0$ , which is far from the center of the distribution of the initial coherent state, as well as most of its width. As for the corresponding case with initial Fock state  $|0, g\rangle$ , the evolution of the NQRM in the coherent state case, depicted in Fig. 10, never exceeds the barrier.

*Conclusions.*—We have proposed the implementation of nonlinear quantum Rabi models, for arbitrary coupling regimes, with trapped-ion analog quantum simulators. The nonlinear term that appears in our model is characteristic for the region beyond the Lamb-Dicke regime.

The nonlinear term causes the blockade of motional propagation at  $|n\rangle$ , whenever  $f_1(a^\dagger a)|n\rangle = 0$ . To compare and contrast our models with standard linear quantum Rabi models, we have firstly plotted the probability distribution and phonon statistics at different times of the linear Jaynes-Cummings model with/without spontaneous decay and the linear quantum Rabi model in the deep strong coupling regime. We have proposed the application of a single trapped-ion system as a large Fock-state generator in the nonlinear Jaynes-Cummings model and as a motional filter in the nonlinear quantum Rabi

model in the DSC regime. Our work sheds new light in the field of nonlinear quantum Rabi models implemented with trapped ions, and suggests plausible applications.

*Acknowledgements.*—The authors acknowledge support from the Chinese Scholarship Council (201506890077), NSFC (11474193), the Shuguang Program (14SG35), the Program for Eastern Scholar, the Basque Government with PhD grant PRE-2015-1-0394 and grant IT986-16, Ramón y Cajal Grant RYC-2012-11391, and MINECO/FEDER FIS2015-69983-P.

- 
- [1] I. I. Rabi, “On the process of space quantization”, *Phys. Rev.* **49**, 324 (1936).
- [2] D. Braak, Q.-H. Chen, M. T. Batchelor, and E. Solano, “Semi-classical and quantum Rabi models: in celebration of 80 years”, *J. Phys. A: Math. Theor.* **49**, 300301 (2016).
- [3] D. Braak, “Integrability of the Rabi Model”, *Phys. Rev. Lett.* **107**, 100401 (2011).
- [4] E. T. Jaynes and F. W. Cummings, “Comparison of quantum and semi-classical radiation theories with application to beam maser”, *Proc. IEEE* **51**, 89 (1963).
- [5] W. P. Schleich, “Quantum Optics in Phase Space”, Wiley (2001).
- [6] D. Leibfried, R. Blatt, C. Monroe, and D. Wineland, “Quantum Dynamics of Single Trapped Ions”, *Rev. Mod. Phys.* **75**, 281 (2003).
- [7] A. A. Houck, H. E. Türeci, and J. Koch, “On-chip Quantum Simulation with Superconducting Circuits”, *Nat. Phys.* **8**, 292 (2012).
- [8] J. M. Raimond, M. Brune, and S. Haroche, “Manipulating quantum entanglement with atoms and photons in a cavity”, *Rev. Mod. Phys.* **73**, 565 (2001).
- [9] A. Moroz, “A hidden analytic structure of the Rabi model”, *Ann. Phys. (N.Y.)* **340**, 252 (2014).
- [10] T. Niemczyk, F. Deppe, H. Huebl, E. P. Menzel, F. Hocke, M. J. Schwarz, J. J. García-Ripoll, D. Zueco, T. Hümmer, E. Solano, A. Marx, and R. Gross, “Circuit quantum electrodynamics in the ultrastrong-coupling regime”, *Nat. Phys.* **6**, 772 (2010).
- [11] P. Forn-Díaz, J. Lisenfeld, D. Marcos, J. J. García-Ripoll, E. Solano, C. J. P. M. Harmans, and J. E. Mooij, “Observation of the Bloch-Siegert Shift in a Qubit-Oscillator System in the Ultrastrong Coupling Regime”, *Phys. Rev. Lett.* **105**, 237001 (2010).
- [12] J. Casanova, G. Romero, I. Lizuain, J. J. García-Ripoll, and E. Solano, “Deep Strong Coupling Regime of the Jaynes-Cummings Model”, *Phys. Rev. Lett.* **105**, 263603 (2010).
- [13] S. De Liberato, “Light-Matter Decoupling in the Deep Strong Coupling Regime: The Breakdown of the Purcell Effect”, *Phys. Rev. Lett.* **112**, 016401 (2014).
- [14] D. Z. Rossatto, C. J. Villas-Bôas, M. Sanz, and E. Solano, “Spectral classification of coupling regimes in the quantum Rabi model”, *Phys. Rev. A* **96**, 013849 (2017).
- [15] M.-J. Hwang, R. Puebla, and M. B. Plenio, “Quantum Phase Transition and Universal Dynamics in the Rabi Model”, *Phys. Rev. Lett.* **115**, 180404 (2015).
- [16] Z.-J. Ying, M.-X. Liu, H.-G. Luo, H.-Q. Lin, and J. Q. You, “Ground-state phase diagram of the quantum Rabi model”, *Phys. Rev. A* **92**, 053823 (2015).
- [17] R. Puebla, M.-J. Hwang, and M. B. Plenio, “Excited-state quantum phase transition in the Rabi model”, *Phys. Rev. A* **94**, 023835 (2016).
- [18] L. Henriët, Z. Ristivojević, P. P. Orth, and K. Le Hur, “Quantum dynamics of the driven and dissipative Rabi model”, *Phys. Rev. A* **90**, 023820 (2014).
- [19] L.-H. Du, X.-F. Zhou, Z.-W. Zhou, X.-X. Zhou, and G.-C. Guo, “Generalized Rabi model in quantum-information processing including the  $A^2$  term”, *Phys. Rev. A* **86**, 014303 (2012).
- [20] Q.-T. Xie, S. Cui, J.-P. Cao, L. Amico, and H. Fan, “Anisotropic Rabi model”, *Phys. Rev. X* **4**, 021046 (2014).
- [21] A. Moroz, “Generalized Rabi models: diagonalization in the spin subspace and differential operators of Dunkl type”, *Europhys. Lett.* **113**, 50004 (2016).
- [22] J. Casanova, R. Puebla, H. Moya-Cessa, and M. B. Plenio, “Equivalence Among Generalized nth Order Quantum Rabi Models”, arXiv:1709.02714.
- [23] S. A. Chilingaryan and B. M. Rodríguez-Lara, “The quantum Rabi model for two qubits”, *J. Phys. A: Math. Theor.* **46**, 335301 (2013).
- [24] L. Lamata, “Digital-analog quantum simulation of generalized Dicke models with superconducting circuits”, *Sci. Rep.* **7**, 43768 (2017).
- [25] L. Garbe, I. L. Egusquiza, E. Solano, C. Ciuti, T. Coudreau, P. Milman, and S. Felicetti, “Superradiant phase transition in the ultrastrong coupling regime of the two-photon Dicke model”, *Phys. Rev. A* **95**, 053854 (2017).
- [26] D. Barberena, L. Lamata, and E. Solano, “Dispersive Regimes of the Dicke Model”, *Sci. Rep.* **7**, 8774 (2017).
- [27] F. Altintas, A. Ü. C. Hardal, and Ö. E. Müstecaplıoğlu, “Rabi model as a quantum coherent heat engine: From quantum biology to superconducting circuits”, *Phys. Rev. A* **91**, 023816 (2015).
- [28] S. Felicetti, E. Rico, C. Sabin, T. Ockenfels, J. Koch, M. Leder, C. Grossert, M. Weitz, and E. Solano, “Quantum Rabi model in the Brillouin zone with ultracold atoms”, *Phys. Rev. A* **95**, 013827 (2017).
- [29] A. Mezzacapo, U. Las Heras, J. S. Pedernales, L. DiCarlo, E. Solano, and L. Lamata, “Digital Quantum Rabi and Dicke Models in Superconducting Circuits”, *Sci. Rep.* **4**, 7482 (2014).
- [30] J. S. Pedernales, I. Lizuain, S. Felicetti, G. Romero, L.

- Lamata, and E. Solano, “Quantum Rabi Model with Trapped Ions”, *Sci. Rep.* **5**, 15472 (2015).
- [31] C. Huerta Alderete and B. M. Rodríguez-Lara, “Cross-cavity quantum Rabi model”, *J. Phys. A: Math. Theor.* **49**, 414001 (2016).
- [32] R. Puebla, J. Casanova, and M. B. Plenio, “A robust scheme for the implementation of the quantum Rabi model in trapped ions”, *New J. Phys.* **18**, 113039 (2016).
- [33] R. Blatt and C. F. Roos, “Quantum Simulations with Trapped Ions”, *Nat. Phys.* **8**, 277 (2012).
- [34] K. Kim, M.-S. Chang, S. Korenblit, R. Islam, E.E. Edwards, J. K. Freericks, G.-D. Lin, L.-M. Duan, and C. Monroe, “Quantum Simulation of Frustrated Ising Spins with Trapped Ions”, *Nature* **465**, 590 (2010).
- [35] J. Casanova, L. Lamata, I. L. Egusquiza, R. Gerritsma, C. F. Roos, J. J. García-Ripoll, and E. Solano, “Quantum Simulation of Quantum Field Theories in Trapped Ions”, *Phys. Rev. Lett.* **107**, 260501 (2011).
- [36] J. Casanova, A. Mezzacapo, L. Lamata, and E. Solano, “Quantum Simulation of Interacting Fermion Lattice Models in Trapped Ions”, *Phys. Rev. Lett.* **108**, 190502 (2012).
- [37] A. Mezzacapo, J. Casanova, L. Lamata, and E. Solano, “Digital Quantum Simulation of the Holstein Model in Trapped Ions”, *Phys. Rev. Lett.* **109**, 200501 (2012).
- [38] L. Lamata, A. Mezzacapo, J. Casanova, and E. Solano, “Efficient Quantum Simulation of Fermionic and Bosonic Models in Trapped Ions”, *EPJ Quantum Technology* **1**, 9 (2014).
- [39] L. Lamata, J. León, T. Schätz, and E. Solano, “Dirac Equation and Quantum Relativistic Effects in a Single Trapped Ion”, *Phys. Rev. Lett.* **98**, 253005 (2007).
- [40] R. Gerritsma, G. Kirchmair, F. Zähringer, E. Solano, R. Blatt, and C. F. Roos, “Quantum Simulation of the Dirac Equation”, *Nature* **463**, 68 (2010).
- [41] R. Gerritsma, B. P. Lanyon, G. Kirchmair, F. Zähringer, C. Hempel, J. Casanova, J. J. García-Ripoll, E. Solano, R. Blatt, and C. F. Roos, “Quantum Simulation of the Klein Paradox with Trapped Ions”, *Phys. Rev. Lett.* **106**, 060503 (2011).
- [42] J. Casanova, C. Sabín, J. León, I. L. Egusquiza, R. Gerritsma, C. F. Roos, J. J. García-Ripoll, and E. Solano, “Quantum Simulation of the Majorana Equation and Unphysical Operations”, *Phys. Rev. X* **1**, 021018 (2011).
- [43] X. Zhang, Y. Shen, J. Zhang, J. Casanova, L. Lamata, E. Solano, M.-H. Yung, J.-N. Zhang, and K. Kim, “Time Reversal and Charge Conjugation in an Embedding Quantum Simulator”, *Nat. Commun.* **6**, 7917 (2015).
- [44] X.-H. Cheng, U. Alvarez-Rodríguez, L. Lamata, X. Chen, and E. Solano, “Time and spatial parity operations with trapped ions”, *Phys. Rev. A* **92**, 022344 (2015).
- [45] I. Arrazola, J. S. Pedernales, L. Lamata, and E. Solano, “Digital-Analog Quantum Simulation of Spin Models in Trapped Ions”, *Sci. Rep.* **6**, 30534 (2016).
- [46] X.-H. Cheng, I. Arrazola, J. S. Pedernales, L. Lamata, X. Chen, and E. Solano “Switchable Particle Statistics with an Embedding Quantum Simulator”, *Phys. Rev. A* **95**, 022305 (2017).
- [47] W. Vogel and R. L. de Matos Filho, “Nonlinear Jaynes-Cummings dynamics of a trapped ion”, *Phys. Rev. A* **52**, 4214 (1995).
- [48] G. Morigi, J. I. Cirac, M. Lewenstein, and P. Zoller, “Ground-state laser cooling beyond the Lamb-Dicke limit”, *Europhys. Lett.* **39**, 13 (1997).
- [49] R. L. de Matos Filho and W. Vogel, “Nonlinear coherent states”, *Phys. Rev. A* **54**, 4560 (1996).
- [50] R. L. de Matos Filho and W. Vogel, “Quantum Nondemolition Measurement of the Motional Energy of a Trapped Atom”, *Phys. Rev. Lett.* **76**, 4520 (1996).
- [51] D. Stevens, J. Brochard, and A. M. Steane, “Simple experimental methods for trapped-ion quantum processors”, *Phys. Rev. A* **58**, 2750 (1998).
- [52] G. Morigi, J. Eschner, J. I. Cirac, and P. Zoller, “Laser cooling of two trapped ions: Sideband cooling beyond the Lamb-Dicke limit”, *Phys. Rev. A* **59**, 3797 (1999).
- [53] M. Fleischhauer and W. P. Schleich, “Revivals made simple: Poisson summation formula as a key to the revivals in the Jaynes-Cummings model”, *Phys. Rev. A* **47**, 4258 (1993).
- [54] D. Ceperley and B. Alder, “Quantum monte carlo”, *Science* **231**, 555 (1986).
- [55] C. F. Lo, “Nonlinear multiquantum Jaynes-Cummings model with counter-rotating terms”, *Quantum Semiclass. Opt.* **10**, L57 (1998).